International Journal of Automotive Technology, Vol. 8, No. 5, pp. 659–666 (2007)

1229–9138/2007/036–15

3-D THERMAL-HYDRAULIC ANALYSIS FOR AIRFLOW OVER A RADIATOR AND ENGINE ROOM

C.-T. HSIEH and J.-Y. JANG*

Department of Mechanical Engineering, National Cheng Kung University,
No.1, University Road, Tainan 70101, Taiwan

(Received 10 April 2007; Revised 9 August 2007)

ABSTRACT–In the present study, a numerical analysis of the three-dimensional heat transfer and fluid flow for a vehicle cooling system was developed. The flow field of the engine room between the grille and radiator was analyzed. The results show that, as the airflow inlet grille angle α is varied from 15° to −15°, the air flow rate compared with α=0° (horizontal) changes from −11.9% to +5.1%; while the heat flux from the radiator changes from −9.2% to +4.4%. When the airflow inlet bumper angle β is varied from −5° to +15°, the heat flux from the radiator compared with β=0° (horizontal) increases up to +4.4%. When the airflow inlet grille angle α=−15° and the bumper grill angle β=+15°, the airflow rates and heat flux compared with (α=0°, β=0°) can be increased to +9.5% and +7.5%, respectively. The results indicate that the optimal angles for cooling efficiency are used.

KEY WORDS : Heat transfer, Radiator, Thermal engineering, CFD, Numerical simulations, 3-D

NOMENCLATURE

k	: thermal conductivity (W/m °C)
$\dot{m}$	: mass flow rate (kg/sec)
p	: pressure
P_r	: Prandtl number
T_w	: wall temperature (°C)
T_b	: bulk mean temperature (°C)
T_{in}	: inlet temperature (°C)
U_i,U_j	: dimensionless velocity vectors
u_i, u_j	: dimensionless fluctuation velocity
u_{in}	: frontal velocity (m/sec)
α	: inlet angle of grille, (°)
β	: inlet angle of bumper grille, (°)
ρ	: density of fluid (kg/m^3)
υ	: kinematics viscosity (m^2/s)

1. INTRODUCTION

An automobile engine takes energy from fuel and converts it into a form of power. The power is used to propel the vehicle. The engine generates temperatures up to 2,500°C of heat within the combustion chamber, but not all of this thermal energy is converted to power. Approximately 25% of this energy is used to push the vehicle. About 9% of the heat generated by the fuel is lost through radiation, and 33% is sent out through the exhaust system. The remaining 33% must be removed by the cooling system (Schwaller, 1999).

In liquid-cooled engines, coolant is pumped throughout the water jacket of the engine, drawing heat from the head, pistons, combustion chambers, cylinder walls, valves, etc. The heated coolant travels from the water jacket through a radiator hose to the radiator, where it is cooled by air and then returns, via the other radiator hose, to the engine. Upon engine start-up, the engine temperature rises quickly. If the engine temperature is too high or too low, various problems will occur. These include overheating of the lubricating oil and engine parts, excessive stresses between engine parts, loss of power, incomplete burning of fuel, etc. These cause fuel to be wasted, and the engine life is shortened.

In automotive engineering, a grille is an opening in the bodywork of a vehicle to allow air to enter. Most vehicles feature a grille at the front of the vehicle to allow air to flow over the radiator and cool the engine compartment. Another common grille location is just below the front bumper. The efficiency of the vehicle cooling system strongly depends on the airflow through the radiator. The flow through the radiator depends on the airflow inlet angles for the grille and bumper.

Recently, due to the rapid development of computing power and numerical techniques, CFD procedures have been adopted as a design tool by many automobile engineers. A number of CFD studies have been carried out regarding heat transfer augmentation. Lee *et al.*

**Corresponding author.* e-mail: jangjim@mail.ncku.edu.tw

(2000) analyzed engine cooling, including flow nonuniformity over a radiator. Yang *et al.* (2002, 2003) applied the CFRM concept to vehicles' thermal systems. Witry *et al.* (2005) used CFD codes to estimate the thermal performance of an automotive aluminium plate radiator. Hsieh *et al.* (2005) carried out a 3-D thermal-hydraulic analysis for louver fin heat exchangers. Lee and Cho (2006) used a numerical analysis procedure to predict the temperature of clutch. However, there are very few studies concerning the effect of the inlet airflow angle on the automotive grille and bumper.

Using computational fluid dynamics (CFD), this paper models the flow and heat transfer performance characteristics for one replacement design for the conventional automotive radiator. A few commercial CFD codes now available are proven to be good for engineering purposes as long as the computational grid and numerical schemes are carefully chosen. In this study, a numerical analysis on the three-dimensional heat and fluid flow of a vehicle's cooling system is presented. Flow is incompressible and has no viscous dissipation; the effects of turbulence are simulated by the k–ε extended turbulence model. The flow field of the engine room between the grille and radiator is also analyzed. The system pressure drop, outlet temperature variation and effect of radiator cooling efficiency for different airflow inlet angles of the grille are investigated. In addition, the airflow rates through the radiator ventilation outlets and the heat flux from the radiator are predicted. The effects of different inlet airflow angles of the grille and bumper are investigated in detail.

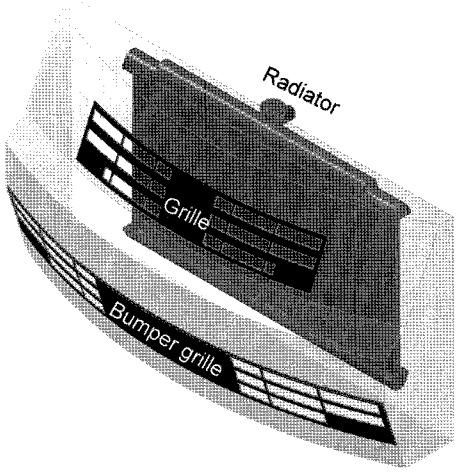

Figure 1. The physical model.

2. MATHEMATICAL ANALYSIS

2.1. Physical Model and Computational Domain

The actual region of the engine room between the grille and radiator, crowded with various engine parts (such as pipelines, electric wires, sensors, frames etc.), is very complicated. In order to simulate this problem conveniently, simplified assumptions and geometric modeling are necessary. Figure 1 shows the physical model, where the 3D computational domain is a complete elementary pattern of the actual automotive shape in the engine room between the grille and radiator. The airflow enters the domain from the ventilation inlets of the grille and bumper. It then passes the engine room space and exits through radiator ventilation outlets. Figure 2 shows the

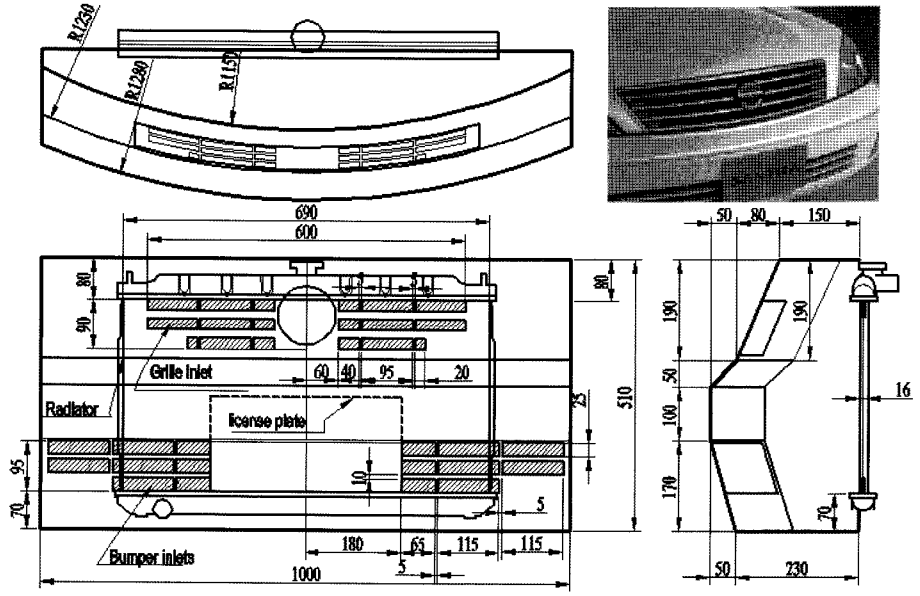

Figure 2. The multiview drawing for the geometric dimension (unit: mm).

multiview drawing for the simplified geometric dimensions from the actual automotive shape (shown in the photograph at upper right-hand side).

2.2. Governing Equations

The fluid is considered incompressible with constant properties and the flow is assumed to be turbulent, steady and three-dimensional with no viscous dissipation. The dimensionless equations for continuity, momentum (Reynolds-averaged Navier-Stokes equations) and energy may be expressed in tensor form as:

$$\frac{\partial U_i}{\partial X_i}=0 \tag{1}$$

$$\frac{\partial}{\partial X_j}(U_iU_j)=-\frac{\partial P}{\partial X_i}+\frac{1}{\mathrm{Re}}[\nabla^2 U_i]-\frac{\partial}{\partial X_j}(\overline{u_iu_j}) \tag{2}$$

$$\frac{\partial}{\partial X_j}(\Theta U_j)=\frac{1}{\mathrm{RePr}}[\nabla^2\Theta]-\frac{\partial}{\partial X_j}(\overline{u_j\theta}) \tag{3}$$

In the above equations, the average velocity (U) and fluctuation velocity (u) have been nondimensionalized with the uniform inlet velocity u_{in} at the channel inlet, all length coordinates with the ventilation inlet's hydraulic diameter D_h, and the pressure with ρu_{in}^2. The dimensionless average temperature and fluctuation temperature are defined as $\Theta=(T-T_{in})/(T_w-T_{in})$ and $\theta=T/(T_w-T_{in})$. The Reynolds number is $Re=u_{in}D_h/\nu$, where D_h is the hydraulic diameter. P_r is the Prandtl number, which is set equal to 0.71 (for air at 40°C) in the present study. Equation (2) contains Reynolds stresses that are modeled by Chen's extended k–ε turbulence model (Chen and Kim, 1987; Wang and Chen, 1993), where k is the turbulent kinetic energy and ε is the dissipation rate. In Chen's model, the production time-scale as well as the dissipation time-scale is used in closing the ε equation. This extra production time-scale is claimed to allow the energy transfer mechanism of turbulence to respond to the mean strain rate more effectively. This results in an extra constant in the ε equation. As to the velocity distribution in the near-wall region ($y+\geq 11.63$), the following law of the wall (Liakopoulos, 1984) is applied.

$$u^+=\ln\left[\frac{(y^++11)^{4.02}}{(y^{+2}-7.37y^++83.3)^{0.79}}\right]+5.63\tan^{-1}(0.12y^+-0.441)-3.81 \tag{4}$$

where

$$y^+\equiv\frac{\rho u_\tau y}{\mu} \quad \text{and} \quad u_\tau=\sqrt{\frac{\tau_w}{\rho}} \tag{5}$$

2.3. Boundary Conditions

Because the governing equations are elliptic in spatial coordinates, the boundary conditions are required for all boundaries of the computation domain. The airflow enters the domain from the ventilation inlets of the grille and bumper. It then passes the engine-room space and exits through the radiator ventilation outlets. The airflow is drawn by a fan behind the radiator. According to the actual automotive operating situations and the results given in a discussion with a manufaction engineer, at the upstream boundary (inlet), constant pressure P_{in}=atmosphere pressure (1 atm) and temperature T_{in}=20°C are assumed. The pressure of the radiator ventilation outlet is assumed to be P_{out}=−30 Pa (relative to atmosphere pressure). The turbulence intensity at the inlet is set at 10%. From the frontal view, the left-hand side and right-hand side computation domains are symmetrical. In this study, only half of the domain is analyzed. At the symmetrical planes, normal gradients are equal to zero. At the solid surfaces of the radiator, no-slip conditions and constant wall temperature T_w (90°C) are specified. The remaining surfaces (except inlet, outlet, radiator surfaces and symmetrical plane) around the domains are assumed to be adiabatic wall surfaces (Figure 3).

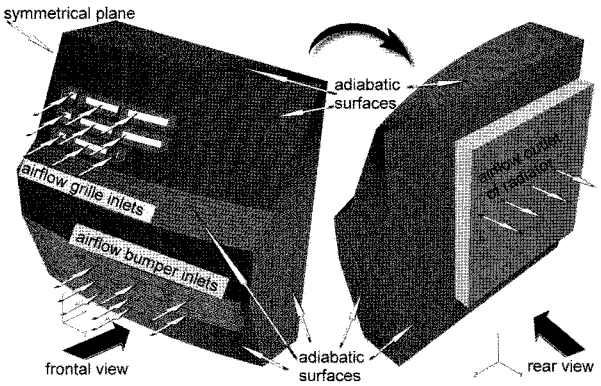

Figure 3. Computational domain and grid system.

2.4. Parameter Definition of Performance Factors

The local pressure drop can be expressed in terms of the dimensionless pressure coefficient Cp defined as

$$Cp=\frac{p_{in}-p}{\frac{1}{2}\rho u_{in}^2} \tag{6}$$

where P_{in} is the pressure at the inlet. The local heat transfer coefficient h is defined as

$$h=\frac{q''}{T_w-T_b} \tag{7}$$

where q'' is the local heat flux and T_b is the local bulk mean temperature of the fluid. The local heat transfer coefficient can be expressed in the dimensionless form by the Nusselt number Nu, defined as

$$Nu=\frac{h\cdot H}{k}=\frac{\partial\left[\frac{\Theta}{\Theta_b}\right]_{wall}}{\partial n} \tag{8}$$

where $\Theta_b=(T_b-T_{in})/(T_w-T_{in})$ is the local dimensionless bulk mean temperature and n is the dimensionless unit vector normal to the wall. The average Nusselt number $\overline{Nu}$ can be obtained by

$$\overline{Nu}=\frac{\int Nu\, dA_s}{\int dA_s} \tag{9}$$

where dA_s is the infinitesimal area of the wall surface.

In order to estimate the heat transfer performance and ventilation efficiency, two parameters are defined as

$$R_{\dot{m}}=(\dot{m}-\dot{m}_o)/\dot{m}_o \tag{10}$$

and

$$R_Q=(Q-Q_o)/Q_o \tag{11}$$

where $\dot{m}$ and Q are, respectively, the mass flow rate and the heat flux at the radiator after the inlet angle is changed. $\dot{m}_o$ and Q_o are, for the base situation, at inlet angle $\alpha=\beta=0°$ (horizontal). In equation (10), $R_{\dot{m}}$ is the ratio between the increased mass flow rate at the radiator $\dot{m}-\dot{m}_o$ and the base mass flow rate $\dot{m}_o$; in equation (11), R_Q is the ratio between the increased heat flux at the radiator Q-Q_o and the base heat flux Q

2.5. Definition of the Geometric Parameters

Figure 4 shows the airflow inlet angle of grille (α) is defined as the angle between the grille's transverse and horizontal planes. When the rear side of the grille's transverse plane is upward, angle α is positive; when it is downward, angle α is negative. In the present study, there are seven cases for various α (α=−15°, −10°, −5°, 0°, +5°, +10°, +15°) investigated.

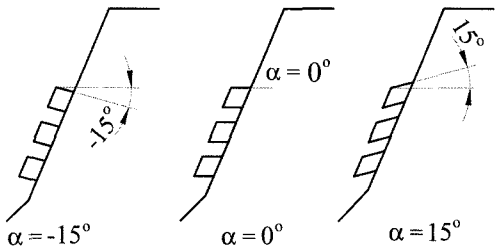

Figure 4 Airflow inlet grille angle (α).

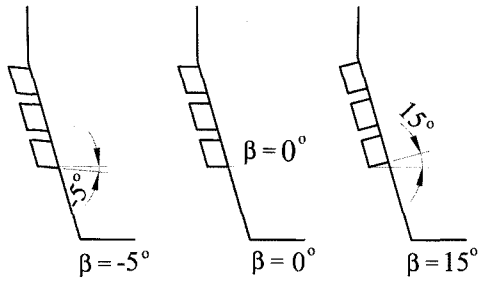

Figure 5. Airflow inlet bumper angle (β).

Figure 5 shows the airflow inlet angle of the bumper (β) is defined as the angle between the bumper grille's transverse and horizontal planes. When the rear side of the bumper grille's transverse plane is upward, angle β is positive; when it is downward, angle β is negative. There are five cases for various β (β=−5°, 0°, +5°, +10°, +15°) investigated in the present study.

3. NUMERICAL METHOD

In this study, the governing equations are solved numerically using a commercial computer program code STAR-CD (2002). The program solves the equations for conservations of mass, momentum and energy using standard finite-volume techniques. This involves subdividing the region in which the flow is to be solved into individual cells or control volumes so that equations can be integrated numerically on a cell-by-cell basis to produce discrete algebraic (finite-volume) equations. A third-order upwind TVD scheme is used to model the convective terms of the governing equations. Second-order central difference schemes are used for the viscous and source terms. For time advancing, an efficient non-iterative time-marching scheme with a predictor/corrector solution algorithm is employed. Several algorithms for calculating the pressure field are available in the program (SIMPLE, PISO, SIMPISO). For these steady-state computations, the SIMPLE algorithm was found to give the shortest computer running times and was used in all of the calculations.

A grid system of 360,231 grid-points is typically adopted in the computation domain, as shown in Figure 3. A careful check for the grid-independence of the numerical solutions has been made to ensure the accuracy and validity of the numerical results. For this purpose, grid systems of 268,576, 360,231 and 482,693 grid-points were tested. It was found that for u_{in}=3.0 m/s, the relative errors in the local pressure and temperature between the solutions of 360,231 and 482,693 grid points are less than 3%. In this paper, all the simulations result from transient calculations, so the steady-state solutions constitute the final states of the transient calculations. Numerically, 'steady-state' is the solution reached when the code has converged, satisfying a criterion of the kind:

$$\frac{\max|\xi^{n+1}-\xi^n|}{\max|\xi^n|}\le\zeta \tag{12}$$

where ξ is U, Θ and P is taken to be compatible with the time-step so that the code marches far enough in time to describe the transient regime before reaching a steady-state. This is done by monitoring the transient evolution of several values, such as the stream function at the centre

Table 1. Cases studied for various α and β

Item	Case studied	Case number
Airflow inlet grille angles α	α=−15°, −10°, −5°, +5°, +10°, +15°	7
Airflow inlet bumper angles β	β=−5°, 0°, +5°, +10°, +15°	5
Different combination for (α, β)	(α, β)=(0°, 0°), (−5°, +5°), (−10°, +10°), (−15°, +15°)	4

of the computational domain. In most cases, for a typical time-step of 10^{-2}, ζ is chosen to be 10^{-7}. All computations were performed on a Pentium IV 3.0G personal computer, typical CPU times were 20 to 26 hours for each case.

4. RESULTS AND DISCUSSIONS

In the present study, the flow field of the engine room between the grille and radiator was analyzed. The system pressure drop, outlet temperature variation and effect of radiator cooling efficiency for different airflow inlet angles of the grille were investigated. The 16 cases of various parameter combinations in the study are tabulated in Table 1. The results and a discussion of them now follow.

4.1. Changes of the Airflow Inlet Grille Angles (α)

In this study, calculations for seven cases were made by changing the grille's airflow inlet angles, for α=−15°, −10°, −5°, 0°, +5°, +10°, +15°. Figure 6 shows the velocity profile for the grille angle α=0°. The fluid flows into the grille inlets and almost directly flows out through the radiator. Most of the fluid flow into the bumper inlets also directly flows out through the radiator. But a little fluid near the side wall follows a longer path before going out through the radiator. This partial fluid often causes a separation or vortex so that the fluid cannot flow out smoothly. Figure 7 shows the streamline distribution for the grille angle α=+15°. A small amount of fluid flow into the grille cannot easily flow out since the grille inlets do not face the outlet. On the contrary, the fluid flow into the grille flows out smoothly for the grille angle α=−15°, as shown in Figure 8. Figure 9 shows the velocity profile for various grille angles (α). The flow moves upward when the grille angle is increased. This phenomenon affects the flow rate and heat transfer performance. Figure 10 shows the air temperature distribution in the radiator outlet for various grille angles. As shown in the

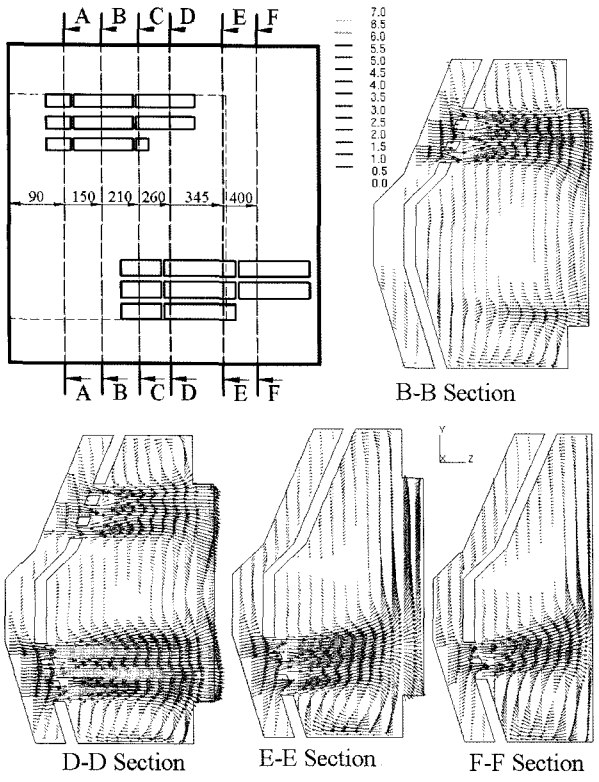

Figure 6. Velocity profile for grille angle α=0°.

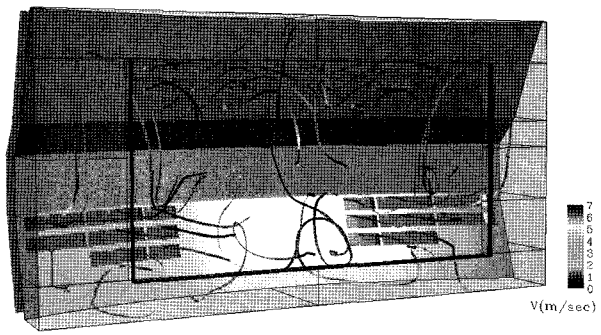

Figure 7. Streamline for grille angle α=+15°.

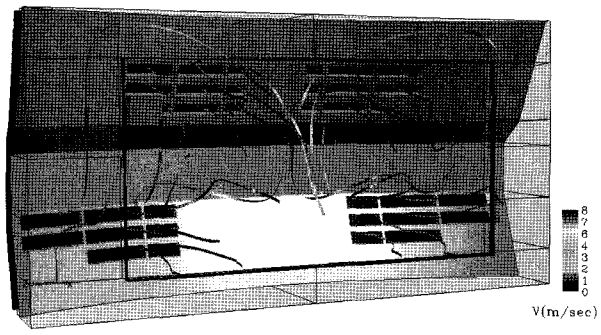

Figure 8. Streamline for grille angle α=−15°.

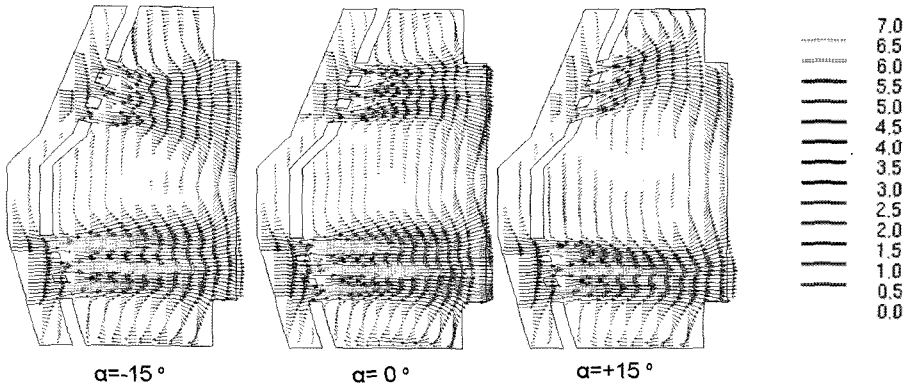

Figure 9. Velocity profile for various α (at C-C section).

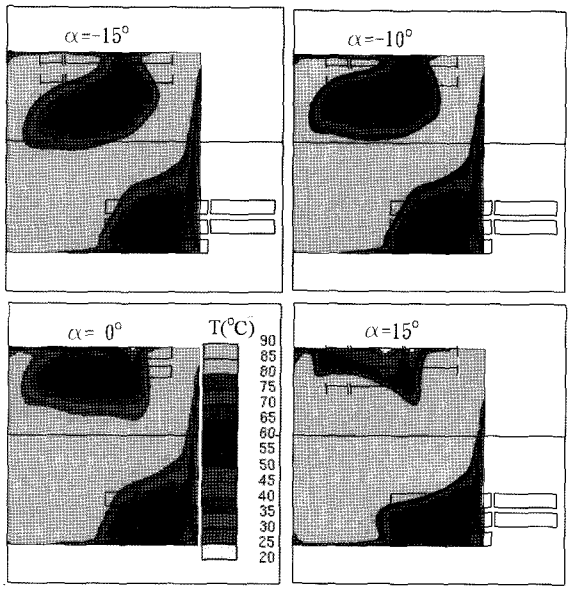

Figure 10. Temperature distribution for various α.

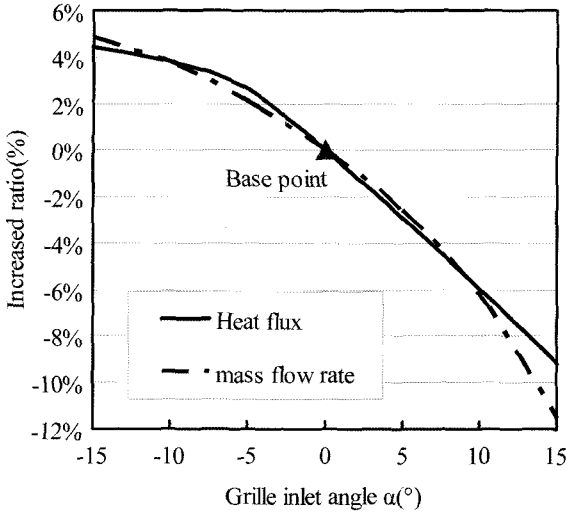

Figure 11. The flow rate and heat flux for various α compare with α=0°.

figures, there are two 'cold zones' that directly receive the impinging flow from the grille and bumper inlets. The velocity in these zones is greater and thus more heat is dissipated.

Figure 11 shows that when the airflow inlet angles of grille (α) are varied from 15° to −15°, the airflow rates compared with α=0° are changed from −11.9% to +5.1%. The heat flux from the radiator compared with α=0° also changes from −9.2% to +4.4%. The results indicated that when the grille's airflow inlet angles, á, decreased, the air flow was more fluent and the mass flow rate increased and carried away more heat. Therefore, heat transfer performance and cooling efficiency are better. However, the angle's decrease is finite. If it decreases too much, the airflow from grille inlets will become so low as to interact with the flow from the bumper grille and become 'choke flow'. The total airflow will not fluently flow through the radiator. According to the results due to the discussion with the grille designer and the actual numerical simulations, in the present study, the angle (α) varied over the range from +15° to −15°.

4.2. Changes of the Airflow Inlet Bumper Angles (β)

In this study, calculations were made for five cases by changing the airflow inlet angles of the bumper, β=−5°, +5°, +10°, +15°. In the case of bumper angle β=−5°, a small amount of fluid flow into the bumper grille cannot fluently flow out because the bumper grille inlets do not face the outlet. In the case of β=+15°, on the contrary, all flow into the grille fluently flows out. This phenomenon affects the flow rate and heat transfer performance. Figure 12 shows the air temperature distribution of the radiator outlet for various bumper grille angles. As seen in the figures, there are two 'cold zones' that directly receive the impinging flow from the grille and bumper inlets. The velocity in these zones is greater and more

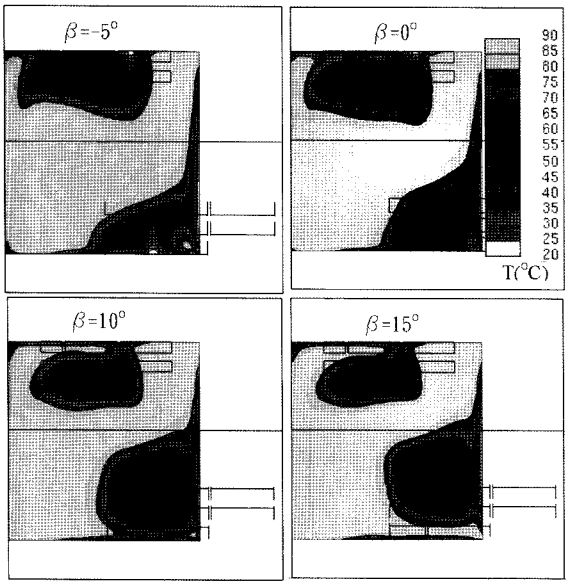

Figure 12. Temperature distribution for various β.

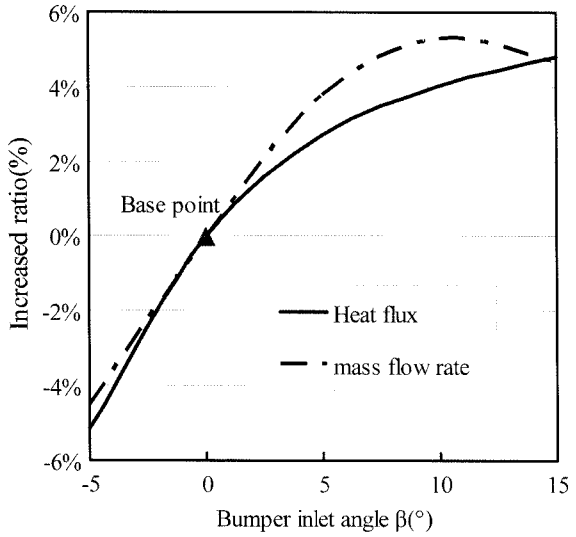

Figure 13. The flow rate and heat flux for various β compared with β=0°.

heat is dissipated. In addition, the lower zone moves up when the bumper grille angle is increased. Figure 13 shows that when the airflow inlet angles of the bumper grille (β) are varied from −5° to +15°, the heat flux from the radiator compared with β=0° is increased to +4.8%. However, the angle's increase is finite. If it increases too much, the air flow from the bumper grille inlets will flow so high as to interact with the flow from the grille and become 'choke flow'. The total airflow will not fluently flow through the radiator. As for the results, the maximum flow rate is +5.3% at β=+10°, but back down to 4.7% at β=+15°. Although the heat flux is still increasing, its proportions are decreased. These results also show that when the airflow is more fluently, the mass flow rate is greater. In other words, there is an 'optimal angle β' in the bumper grille design. For the same reason as stated in the previous section, in the present study, the angles are varied from −5° to +15°.

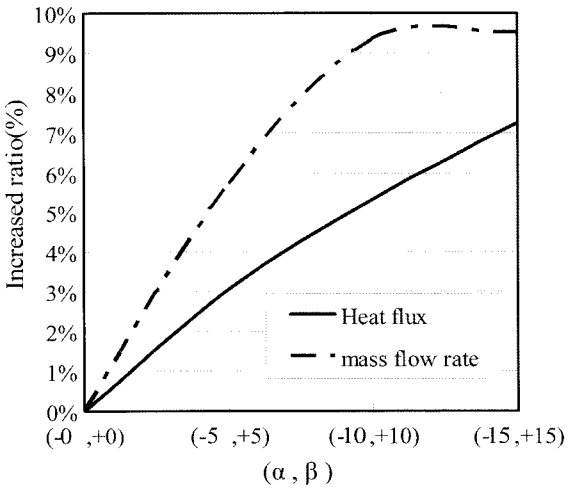

Figure 14. The flow rate and heat flux for various (α, β) compared with (α, β)=(0°, 0°).

4.3. Simultaneously Changing Both the Inlet Grille and Bumper Angles

The above results and discussion provide evidence that both the inlet airflow angles of the grille and bumper affect the flow field and heat transfer performance. Therefore, combining these two factors, for four cases of simultaneously changing both the angle of the grille and of the bumper inlets ((α, β)=(0°, 0°), (−5°, +5°), (−10°, +10°), (−15°, +15°)) are investigated. The airflow and streamline distribution for α=−15° and β=+15° are very complicated. As shown in Figure 14, when the inlet airflow angles of both the grille and bumper are simultaneously changed to α=−15° and β=+15°, the airflow rates compared with β=0° are increased to +9.5%, and the heat flux is also increased to +7.3%. However, there is also a maximum flow rate of +9.7% at β=+12°. Although the heat flux is still increasing, its proportions are cut down. These results indicate that if the inlet airflow angles of both the grille and bumper are changed, there is an 'optimal angle' in the bumper and grille design such that the heat transfer performance and cooling efficiency will be most effective.

5. CONCLUSIONS

3-D fluid flow and heat transfer for the engine room between the grille and radiator are studied numerically. Flow is assumed to be turbulent and three-dimensional,

and a computational domain from the fluid inlet and outlet is solved directly. The system pressure drop, outlet temperature variation and effect of radiator cooling efficiency for different airflow inlet angles of the grille were investigated and compared. Major conclusions are summarized as follows:

(1) When the airflow inlet grille angle (α) is varied from +15° to −15°, the airflow rate compared with α=0° changes from −11.9% to +5.1%, while the heat flux from the radiator changes from −9.2% to +4.4%.
(2) When the airflow inlet bumper angle (β) is varied from −5° to +15°, the heat flux from the radiator compared with β=0° increases to +4.8%. However, there is a maximum flow rate of +5.3% at β=+10°; the results indicated that an 'optimal angle β' in the bumper grille design exists.
(3) When the airflow inlet grille angle α=−15° and bumper grill angle β=+15°, airflow rates and heat flux compared with (α=0°, β=0°) can be increased to +9.5% and +7.5%, respectively. A maximum flow rate of +9.7% is found at α=−12°, β=+12°.

The results indicate that if both the inlet grill and the bumper airflow angles are changed, there is an 'optimal angle' in the bumper and grille design, at which angle the cooling efficiency is most effective. The conclusions of this research will also be a valuable reference for the automotive manufaction engineer and bumper grille designer.

ACKNOWLEDGEMENTS–The financial support for this study was provided by Yen Tjing Ling Industrial Research Institute. The authors also wish to express their gratitude to Mr. C. P Wang and Mr. R. C. Tu of Yulon Nissan Motor Co., Ltd. for their assistance to this paper.

REFERENCES

Chen, Y. S. and Kim, S. W. (1987). Computation of turbulent flows using an extended k-ε turbulence closure model, NASA CR-179204.

Hsieh, C. T. and Jang, J. Y. (2006). 3-D thermal-hydraulic analysis for louver fin heat exchangers with variable louver angle. *Applied Thermal Engineering,* **26**, 1629–1639.

Lee, B. and Cho, C. (2006). Numerical analysis procedure for predicting temperature field in design of automotive friction clutch. *Int. J. Automotive Technology* **7**, **1**, 61–68.

Lee, Y. L. and Hong, Y. T. (2000). Analysis of engine cooling including flow nonuniformity over a radiator. *Int. J. Vehicle Design (IJVD)*, **24**, **1**, 121–135.

Liakopoulos, A. (1984). Explicit representations of the complete velocity profile in a turbulent boundary layer. *AIAA J.*, **22**, 844–846.

Schwaller, A. E. (1999). *Motor Automotive Technology.* 3rd edn.. Delmar Publishers. New York.

STAR CD V.3.15A (2002). *Simulation of Turbulent Flow in Arbitrary Regions*. Computional Dynamics Limited. UK.

Wang, T. S. and Chen, Y. S. (1993). Unified navier-stokes flow field and performance analysis of liquid rocket engines, *AIAA J.* **9**, **5**, 678–685.

Witry, A., Al-Hajeri, M. H. and Bondok, A. A. (2005). Thermal performance of automotive aluminum plate radiator. *Applied Thermal Engineering,* **25**, 1207–1218.

Yang, Z., Boseman, J., Shen, F. Z. and Acre, J. A. (2002). CFRM concept for vehicle thermal system. *SAE Paper No.* 2002-01-1207.

Yang, Z., Boseman, J., Shen, F. Z. and Acre, J. A. (2003). CFRM concept at vehicle idle conditions. *SAE Paper No.* 2003-01-0613.